Boundary Conditions on Conical Hydrophobic Inclusions in Lipid Membranes

Sina Zendehroud,[1] Philip Loche,[1] Ralf Kornhuber,[2] and Roland R. Netz[1]

[1] *Freie Universität Berlin, Department of Physics, Arnimallee 14, 14195 Berlin, Germany*
[2] *Freie Universität Berlin, Department of Mathematics and Computer Science, Arnimallee 6, 14195 Berlin, Germany*

(Dated: January 13, 2022)

Using all-atom Molecular Dynamics simulations including explicit water, we consider hydrophobic inclusions of conical shape that are inserted into phospholipid bilayer membranes with the goal to determine the boundary conditions at the inclusion-membrane interface. We determine the mean membrane shape around the inclusion and from that extract the membrane vertical-displacement, thickness and bending-angle profiles as possible order parameters in a coarse-grained description of the membrane shape. Via comparison with solutions of membrane-shape equations obtained by Landau theory, we investigate the appropriate boundary condition at the inclusion-membrane interface. We find that in the considered cone opening angle range, the boundary values of the different order parameters that describe the membrane deformation are rather constant, which reflects an inherently preferred shape of membranes at conical inclusions.

I. INTRODUCTION

Cell membranes are barriers that separate the cytoplasm inside the cell from the outside extracellular fluid and at the same time allow the formation of intracellular compartments. They are thus an integral part of the biological machinery enabling life [1].

On the microscopic scale, cell membranes typically consist of a mixture of different lipids and membrane proteins. As pure lipid bilayers resist spontaneous bending due to their elastic properties [2, 3], molecular mechanisms are needed to introduce curvature to the membrane. Curvature generation by inclusions and scaffold proteins have been reported in many experimental studies, see e.g. Refs. [4–8]. It is useful to differentiate internal membrane bending mechanisms, due to the asymmetric insertion of amphipathic helices or the insertion of wedge-shaped transmembrane proteins into the bilayer, from external bending mechanisms, where curvature is introduced by proteins that adsorb onto the bilayer, such as binding of the intrinsically curved Bin-Amphiphysin-Rvs (BAR) domain protein superfamily [3, 9]. In the present work, we consider hydrophobic transmembrane inclusions of conical shape, which may be considered as a simple model of internal membrane bending. A recent computational study of membrane sculpting by BAR domains is found in Ref. [10]. Membrane curvature generation by asymmetric insertion of amphipathic helices has been recently studied in Ref. [11], hydrophobic transmembrane insertions have been considered in Ref. [12].

On the macroscopic scale, continuum models based on the pivotal Canham-Helfrich model of lipid membranes [13, 14] have been used to study large-scale effects of inclusions on membrane shape, see also Refs. [15, 16]. In the Canham-Helfrich model, the equilibrium membrane shape follows from minimizing the associated energy functional, which is obtained by expansion of the bending energy with respect to the principal curvatures up to second order. Modifications of this model include effects of different lipid components or protein assemblies via areal concentrations [17, 18]. Since microscopic descriptions, usually based on Molecular Dynamics (MD) simulations, have certain limitations regarding the accessible time and length scales, while continuum descriptions do not incorporate the effects of discrete particles, hybrid approaches attempt to bridge the gap between microscopic and macroscopic descriptions [19–21]. In principle, the idea is to model the coupling between a protein and the membrane microscopically and infer suitable boundary conditions at the protein-membrane interface, which can then be used in continuum descriptions. A mathematically consistent formulation of a variety of models with regard to hybrid approaches and numerical accessibility can be found in Ref. [22].

In the present work, we perform atomistic simulations of purely hydrophobic transmembrane inclusions of conical shape in double lipid membranes and utilize the phenomenological framework of Landau theory [23] to study the coupling of the inclusion to the membrane. Landau theory has been used successfully before to describe various effects connected to the shape of lipid membranes [24–28]. Conical inclusions are of particular interest, because they represent typical wedge-shaped membrane proteins and have been previously considered in Refs. [20, 26, 29, 30].

The organization of this paper is as follows. In Sec. II, we introduce our phenomenological theory and minimize the Landau free energy in polar coordinates in the presence of boundary fields. We obtain a system of ordinary differential equations that predict the behavior of general scalar order parameters including the boundary to the conical inclusion which describe the membrane shape. In Sec. III, we describe our simulation protocol and the extraction of order parameters from simulation data. In Sec. IV, we compare our theory to explicit order parameters from atomistic simulations and infer the boundary conditions in the theoretical model using simulation data. Finally, in Sec. V, we close with some concluding remarks.

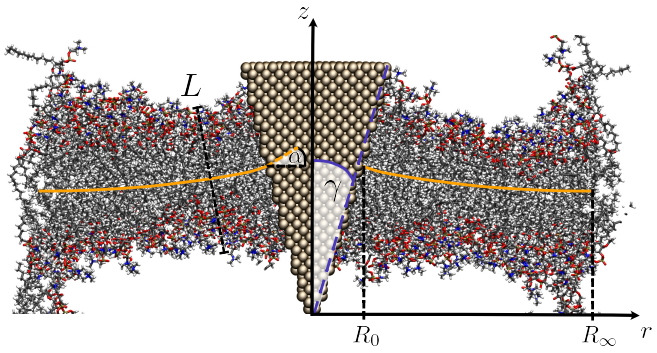

FIG. 1. Snapshot of our simulation setup showing the lipid bilayer membrane with a conical insertion of half opening angle $\gamma = 15°$. The figure shows a cut through the center of the cone. The membrane middle plane is indicated by an orange line, and definitions of membrane thickness L, middle plane bending angle α and cone half opening angle γ are shown. The water molecules surrounding cone and membrane are not shown.

II. ORDER PARAMETER DESCRIPTION

The membrane shape perturbation due to the presence of a conical hydrophobic inclusion is described within a general scalar Landau theory in terms of a spatially-dependent order parameter $\eta(r)$, while the effects of the inclusion enter via surface boundary conditions.

We expand the free energy of the lipid membrane in terms of the scalar order parameter $\eta(r)$ according to the Landau theory [23] in polar coordinates. We assume that the inclusion tip is located at $r = 0$, and position the inclusion-membrane interface defined at the membrane middle plane at $r = R_0$, see Fig. 1. Considering only the lowest-order terms and including interface effects via boundary fields $h_\pm$ and $g_\pm$, which couple linearly and quadratically, respectively, to the order parameter values at $r = R_0$ and $r = R_\infty$, the edge of the simulation box, the free energy can be written as

$$\begin{aligned}\frac{\mathcal{F}[\eta(\cdot)]}{\mathcal{L}} = 2\pi \int_{R_0}^{R_\infty} \left[a\eta^2(r) + c\left(\frac{\mathrm{d}\eta(r)}{\mathrm{d}r}\right)^2 \right] r\ \mathrm{d}r \\ + 2\pi R_\infty h_+ \eta(R_\infty) + 2\pi R_0 h_- \eta(R_0) \\ + 2\pi R_\infty g_+ \eta^2(R_\infty) + 2\pi R_0 g_- \eta^2(R_0)\ . \end{aligned} \tag{1}$$

Here a and c are phenomenological parameters, measuring the stiffness of the order parameter and the spatial range of interactions, respectively, and $\mathcal{L}$ is the mean thickness of the membrane.

Following the variational principle, the free energy Eq. (1) is minimized by

$$\frac{\delta\mathcal{F}[\eta(\cdot)]}{\delta\eta(\tilde{r})} = 0\ , \tag{2}$$

leading to

$$r^2\eta''(r) + r\eta'(r) - \frac{a}{c}r^2\eta(r) = 0 \tag{3}$$

$$h_+ + 2g_+\eta(R_\infty) + 2c\eta'(R_\infty) = 0 \tag{4}$$

$$h_- + 2g_-\eta(R_0) + 2c\eta'(R_0) = 0\ . \tag{5}$$

The general solution of Eq. (3) is

$$\eta(r) = k_1 I_0(r/\lambda) + k_2 K_0(r/\lambda)\ , \tag{6}$$

where we have defined the correlation length $\lambda := (c/a)^{1/2}$ which describes the range over which order-parameter perturbations relax within the membrane. We denote the modified Bessel functions of the first and second kind by $I_\nu(r)$ and $K_\nu(r)$, $\nu \in \mathbb{N}$, respectively, and k_1, k_2 are scalar parameters to be determined, depending on the boundary condition. In the following, we derive the solutions using Neumann and Dirichlet boundary conditions, respectively.

A. Neumann boundary conditions

If the order parameter is chosen such that it reaches a minimum at R_∞, it is appropriate to use Neumann boundary conditions, i.e., $\eta'(R_\infty) = 0$, leading to

$$\eta(r) = \eta_0 \frac{K_1(R_\infty/\lambda)I_0(r/\lambda) + I_1(R_\infty/\lambda)K_0(r/\lambda)}{I_0(R_0/\lambda)K_1(R_\infty/\lambda) + I_1(R_\infty/\lambda)K_0(R_0/\lambda)}\ , \tag{7}$$

where we have defined the boundary value $\eta_0 := \eta(R_0)$.

Inserting the expression for the order parameter $\eta(r)$ from Eq. (7) into Eq. (4) yields

$$\eta(R_\infty) = \frac{-h_+}{2g_+}\ , \tag{8}$$

which fixes the ratio of the boundary fields h_+ and g_+. These are of minor importance to our analysis, since they describe the coupling of the membrane to the outer boundary, the effect of which on the membrane shape around the inclusion should vanish if the simulation box is chosen large enough.

Inserting the expression for the order parameter $\eta(r)$ from Eq. (7) into Eq. (5), on the other hand, yields

$$\eta_0(\gamma) = -h_- \Big/ \left(2g_- + 2c\lambda^{-1} \frac{I_1(R_0(\gamma)/\lambda)K_1(R_\infty/\lambda) - I_1(R_\infty/\lambda)K_1(R_0(\gamma)/\lambda)}{I_0(R_0(\gamma)/\lambda)K_1(R_\infty/\lambda) + I_1(R_\infty/\lambda)K_0(R_0(\gamma)/\lambda)} \right)\ . \tag{9}$$

Since R_0 is a function of the cone half opening angle γ, Eq. (9) predicts a γ-dependent boundary value $\eta_0(\gamma)$ for

given boundary fields h_-, g_-. This describes the coupling of the membrane to the conical inclusion, which is the main subject of our investigation.

B. Dirichlet boundary conditions

If, on the other hand, the order parameter takes the value zero at R_∞, which would be expected for an order parameter profile that is an odd function between two inclusions, such as the membrane bending angle, it is appropriate to use the Dirichlet boundary condition $\eta(R_\infty) = 0$, leading to

$$\eta(r) = \eta_0 \frac{I_0(R_\infty/\lambda)K_0(r/\lambda) - K_0(R_\infty/\lambda)I_0(r/\lambda)}{I_0(R_\infty/\lambda)K_0(R_0/\lambda) - K_0(R_\infty/\lambda)I_0(R_0/\lambda)} \ . \tag{10}$$

Inserting the expression for the order parameter $\eta(r)$ from Eq. (10) into Eq. (4) yields

$$\eta_0(\gamma) = \frac{h_+}{2c}(I_0(R_\infty/\lambda)K_0(R_0(\gamma)/\lambda) - I_0(R_0(\gamma)/\lambda)K_0(R_\infty/\lambda)) \ . \tag{11}$$

Again, since R_0 is a function of γ, Eq. (11) predicts a γ-dependent boundary value $\eta_0(\gamma)$ with fixed boundary fields h_+, g_+, which are of minor importance since they describe the coupling of the membrane to the outer boundary and the effect should vanish for large systems.

Inserting the expression for the order parameter $\eta(r)$ from Eq. (7) into Eq. (5), on the other hand, yields

$$\eta_0(\gamma) = -h_- / \left(2g_- + 2c\lambda^{-1}\frac{I_0(R_\infty/\lambda)K_1(R_0(\gamma)/\lambda) + I_1(R_0(\gamma)/\lambda)K_0(R_\infty/\lambda)}{I_0(R_\infty/\lambda)K_0(R_0(\gamma)/\lambda) - I_0(R_0(\gamma)/\lambda)K_0(R_\infty/\lambda)}\right) \ . \tag{12}$$

As for the Neumann boundary conditions, since R_0 is a function of γ, Eq. (12) predicts a γ-dependent boundary value $\eta_0(\gamma)$ for given boundary fields h_-, g_-.

III. MOLECULAR DYNAMICS SIMULATIONS

We perform all-atom molecular dynamics (MD) simulations of a DMPC bilayer membrane solvated in water using the CHARMM force-field [31]. Periodic boundaries are employed in all directions, and a time step of $\Delta t = 2\,\mathrm{fs}$ is used. The system contains 648 DMPC lipids as well as 32,400 water molecules and is initially equilibrated for 10 ns in the NpT ensemble. The velocity rescale thermostat [32], including a stochastic factor, is employed with a time constant of 0.5 ps. For the pressure coupling we employ a semi-isotropic Berendsen barostat [33] with a time constant of 1 ps coupled independently in the z and the xy direction. The purely hydrophobic conical inclusions are made of frozen carbon atoms and are cut from an fcc lattice with a lattice constant of 0.3567 nm. The inclusions with half opening angles $\gamma \in \{10°, 12.5°, 15°, 17.5°, 20°\}$ are inserted into the equilibrated pure bilayer system in the middle of the xy-plane, by gradually switching on the interaction potential between the inclusion atoms and all other atoms over a time of 2 ns. The system is subsequently equilibrated in the NpT ensemble for at least 100 ns. To furthermore avoid motion of the membrane, we apply a harmonic force on the center of mass of the lipids in the z direction with a force constant of $1000\,\mathrm{kJ/mol/nm^2}$. We generate production trajectories of at least 100 ns in the NVT ensemble, i.e., the lateral area is fixed to 14 nm × 14 nm in the simulations. The positions of all particles are saved every 20 ps.

The polar coordinate system is constructed such that the tip of the conical inclusion is located at $r = 0$. To extract radial membrane shape profiles, we compute the radial average of the membrane head and tail group positions, respectively, for both the upper and lower leaflet. The radial displacement profile of the membrane middle plane $u(r)$ is then determined as the mean of the two tail group position profiles, and the lipid-cone interface at $r = R_0$ is determined by the maximal value of the middle plane position profile, as shown in Fig. 2 (c), (d) for angles $\gamma = 10°,\ 20°$. The remaining profiles are shown in Fig. 5 in the Appendix. We fit the upper and lower leaflet position profiles, respectively, with a ninth degree polynomial, the middle plane position profile is described by a forth degree polynomial fit. The polynomial fit to the middle plane position profile is only used to ensure that the thickness determined via orthogonal projection is smooth. We furthermore extract the middle plane bending angle $\alpha(r)$ via its radial derivative as well as the membrane thickness $L(r)$ defined as the distance between upper leaflet and lower leaflet profiles orthogonal to the middle plane position, see Fig. 2 and Fig. 5. The extracted cone-lipid interface positions R_0 are shown in Fig. 2 (e) as a function of the cone half opening angle γ. We approximate the dependence of R_0 on γ by a linear fit through the origin of the form $R_0(\gamma) = a\gamma$, shown as a red line in Fig. 2 (e). The fitting parameter is $a = (0.133 \pm 0.002)\,\mathrm{nm}/\,°$.

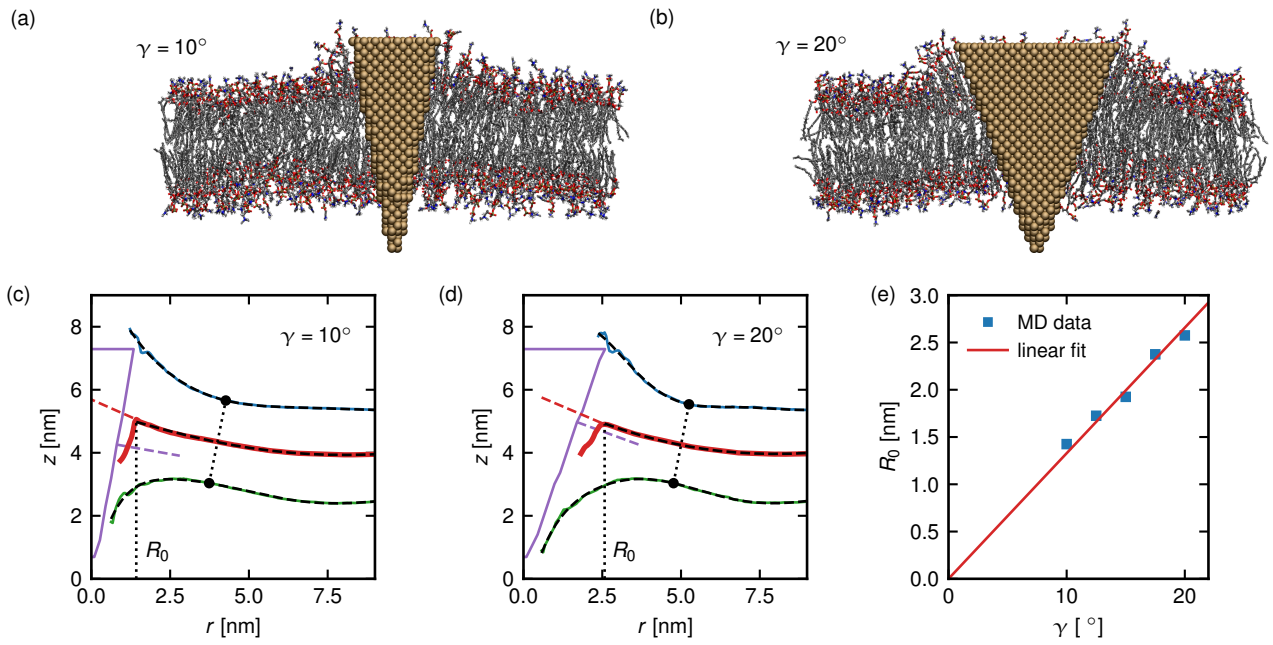

FIG. 2. (a), (b) Simulation snapshots for a conical inclusion of half opening angle $\gamma = 10°$ (a) and $\gamma = 20°$ (b) at the end of the respective trajectories. (c), (d) Radial membrane profiles for $\gamma = 10°$ (c) and $\gamma = 20°$ (d). Extracted radial average of the upper and lower leaflet head group positions as well as the middle plane position are shown as solid lines in color: upper leaflet head group positions in blue, lower leaflet head group positions in green, and middle plane position in red. A tangent to the middle plane position profile at the cone-membrane interface R_0 is shown as a red dashed line. The corresponding polynomial fits are shown as black dashed lines. The conical inclusion is represented by a solid purple line drawn through the outermost atoms' centers of the cone. The purple dashed line is orthogonal to the cone edge profile as a guide to the eye. The lipid cone interface at R_0 is indicated by a black dotted vertical line. The orthogonal projection to the middle plane is shown as a black dotted line, where black filled circles indicate the extracted membrane thickness. (e) Extracted cone-lipid interface positions R_0 as a function of cone half opening angle γ. A linear fit through the origin is shown as a red straight line.

IV. ORDER PARAMETERS IN ATOMISTIC SIMULATIONS

The phenomenological Landau theory described in Sec. II accounts for the energy of the profile of a general order parameter $\eta(r)$. There are many membrane order parameters that may be relevant for the interaction of the membrane with the conical hydrophobic inclusion. Here, we examine three different order parameter profiles from our explicit simulations described in Sec. III. The order parameters we consider are

1. the radial displacement profile of the membrane middle plane position, $\eta^{(1)}(r) = u(r) - u(R_\infty)$ for $r \in [R_0, R_\infty]$, with the Neumann boundary condition $u'(R_\infty) = 0$,

2. the radial dependence of the membrane thickness, $\eta^{(2)}(r) = L(r)$ for $r \in [R_0, R_\infty]$, with the Neumann boundary condition $L'(R_\infty) = 0$,

3. the radial dependence of the middle plane bending angle, $\eta^{(3)}(r) = \alpha(r)$ for $r \in [R_0, R_\infty]$, with the Dirichlet boundary condition $\alpha(R_\infty) = 0$.

We show the profiles of the considered order parameters $\eta^{(1)}$ and $\eta^{(2)}$ together with fits to Eq. (7) in Fig. 3 (a), (b). The profiles of the order parameter $\eta^{(3)}$ together with fits to Eq. (10) are shown in Fig. 4 (a)–(e). The displacement order parameter $\eta^{(1)}$, shown for $\gamma \in \{10°, 12.5°, 15°, 17.5°, 20°\}$ in Fig. 3 (a), is reasonably well described by the theoretical model Eq. (7). Deviations are seen predominantly at the outer boundary R_∞ which is far away from the inclusion, where the theory fails to reproduce that the displacement assumes zero, i.e., the unperturbed state, at R_∞. The fitting parameters are $\lambda^{(1)} = (2.64 \pm 0.07)\,\mathrm{nm}$ and $\eta_0^{(1)} = (1.26 \pm 0.02)\,\mathrm{nm}$ for $\gamma = 10°$, $\lambda^{(1)} = (2.53 \pm 0.07)\,\mathrm{nm}$ and $\eta_0^{(1)} = (1.26 \pm 0.03)\,\mathrm{nm}$ for $\gamma = 12.5°$, $\lambda^{(1)} = (2.41 \pm 0.07)\,\mathrm{nm}$ and $\eta_0^{(1)} = (1.32 \pm 0.03)\,\mathrm{nm}$ for $\gamma = 15°$, $\lambda^{(1)} = (2.17 \pm 0.06)\,\mathrm{nm}$ and $\eta_0^{(1)} = (1.24 \pm 0.02)\,\mathrm{nm}$ for $\gamma = 17.5°$, and $\lambda^{(1)} = (2.01 \pm 0.05)\,\mathrm{nm}$ and $\eta_0^{(1)} = (1.10 \pm 0.02)\,\mathrm{nm}$ for $\gamma = 20°$. Note that the correlation lengths $\lambda^{(1)}$ are all of the same order of magnitude, which is expected since $\lambda^{(1)}$ reflects a bulk membrane property which should not be modified by the cone opening angle. The surface values $\eta_0^{(1)}$ are shown in Fig. 3 (c), and, except for the slight drop at $\gamma = 20°$, do not change much

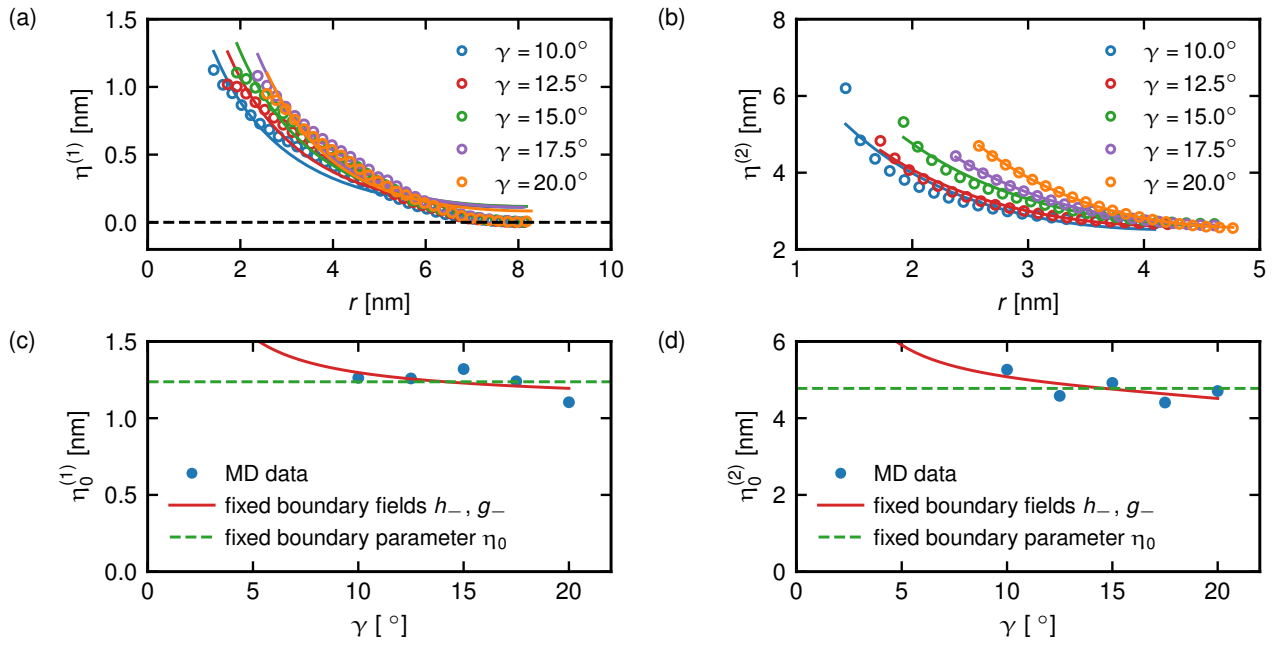

FIG. 3. Membrane order parameter profiles from atomistic simulations (data points) and from Landau theory (lines). (a) Displacement profile of the membrane middle plane position $\eta^{(1)}$ and (b) membrane thickness profile $\eta^{(2)}$. The parameters of the theoretical model Eq. (7) are fitted to the MD data. Panel (c), (d) show the interface values η_0 of the corresponding order parameters obtained in the simulations (data points) together with theoretical predictions according to Eq. (9) (lines).

with the cone half opening angle γ. The fit of $\eta_0^{(1)}$ to Eq. (9) is shown as a solid red line. For the fit, we use $\lambda^{(1)}(20°)$ and determine c as a fitting parameter. We obtain $h_-^{(1)} = -4.4$, $g_-^{(1)} = 2.5$ and $c^{(1)} = 1.0$. We omit the errors of the fit since they are several orders of magnitude higher than the obtained optimal parameters. We see that a boundary model assuming constant surface fields h_- and g_- yields results that are almost identical to assuming a constant boundary value $\eta_0^{(1)}$.

Similarly, the membrane thickness order parameter $\eta^{(2)}$ is shown in Fig. 3 (b). For the cone angles $\gamma = 17.5°$ and $\gamma = 20°$, the theoretical fits describe the MD data very well. For the lower values of γ, the model fails to predict the significant increase in thickness at the inclusion-membrane interface R_0, which might reflect missing higher-order terms in the Landau theory. The fitting parameters are $\lambda^{(2)} = (2.4 \pm 0.1)\,\text{nm}$ and $\eta_0^{(2)} = (5.3 \pm 0.2)\,\text{nm}$ for $\gamma = 10°$, $\lambda^{(2)} = (2.59 \pm 0.04)\,\text{nm}$ and $\eta_0^{(2)} = (4.58 \pm 0.04)\,\text{nm}$ for $\gamma = 12.5°$, $\lambda^{(2)} = (2.59 \pm 0.05)\,\text{nm}$ and $\eta_0^{(2)} = (4.92 \pm 0.06)\,\text{nm}$ for $\gamma = 15°$, $\lambda^{(2)} = (2.38 \pm 0.01)\,\text{nm}$ and $\eta_0^{(2)} = (4.41 \pm 0.01)\,\text{nm}$ for $\gamma = 17.5°$, and $\lambda^{(2)} = (2.11 \pm 0.01)\,\text{nm}$ and $\eta_0^{(2)} = (4.71 \pm 0.01)\,\text{nm}$ for $\gamma = 20°$. Again, the correlation lengths $\lambda^{(2)}$ are all of the same order of magnitude, as expected. The surface values $\eta_0^{(2)}$ are shown in Fig. 3 (d). In contrast to $\eta_0^{(1)}$, a slight γ-dependence can be observed. Again, the fit of $\eta_0^{(2)}$ to Eq. (9) is shown as a solid line. Using the same fitting procedure as in the case of $\eta_0^{(1)}$, we obtain $h_-^{(2)} = -15.4$, $g_-^{(2)} = 2.1$ and $c^{(2)} = 0.8$. We again omit the errors of the fit since they are several orders of magnitude higher than the obtained optimal parameters.

Finally, we show the middle plane bending angle order parameter $\eta^{(3)}$ in Fig. 4 (a)–(e). The bending angle values are calculated using the numerical derivative of the extracted middle plane position profiles and thus exhibit significant scattering due to the high resolution of our data. However, the qualitative radial behavior is reasonably well reproduced by the fits. The fitting parameters are $\lambda^{(3)} = 11.6\,\mu\text{m}$ and $\eta_0^{(3)} = 23.8° \pm 0.9°$ for $\gamma = 10°$, $\lambda^{(3)} = 20.6\,\mu\text{m}$ and $\eta_0^{(3)} = 24.0° \pm 0.6°$ for $\gamma = 12.5°$, $\lambda^{(3)} = 25.9\,\mu\text{m}$ and $\eta_0^{(3)} = 23.6° \pm 0.9°$ for $\gamma = 15°$, $\lambda^{(3)} = 8.3\,\mu\text{m}$ and $\eta_0^{(3)} = 25.14° \pm 0.5°$ for $\gamma = 17.5°$, and $\lambda^{(3)} = 28.95\,\mu\text{m}$ and $\eta_0^{(3)} = 23.1° \pm 0.4°$ for $\gamma = 20°$. In this case, note that the correlation lengths $\lambda^{(2)}$ are in the micrometer range and thus much larger than the simulation system size. We omit the errors of the $\lambda^{(3)}$ fit parameters since they are several orders of magnitude higher than the obtained optimal parameters. The surface values $\eta_0^{(3)}$ are shown in Fig. 4 (f). Similar to $\eta_0^{(1)}$, the boundary parameters $\eta_0^{(3)}$ do not depend on the cone half opening angle γ. We additionally show the axes-bisector as a black dotted line, indicating that the lipid angles at the interface do not simply align to the opening

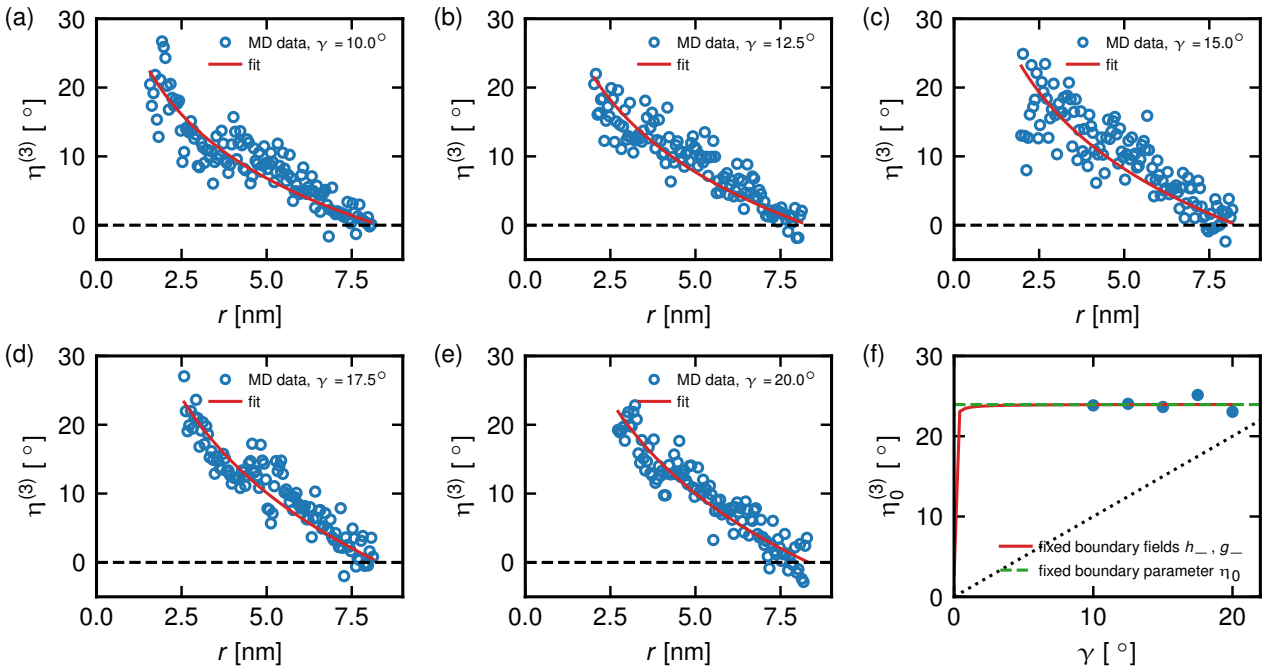

FIG. 4. (a)–(e) Membrane middle plane bending angle profiles $\eta^{(3)}$. The parameters of the theoretical model Eq. (10), the results of which are shown as lines, are fitted to the MD data, shown as data points. Panel (f) shows the interface values $\eta_0^{(3)}$ of the corresponding order parameter obtained in the simulations (data points) together with the theoretical prediction according to Eq. (12) for fixed boundary fields (solid red line) and for a fixed order parameter value (broken green line).

angle of the conical inclusion. As before, the fit of $\eta_0^{(3)}$ to Eq. (12) is shown as a solid line. Similar to the fits shown in Fig. 3 (c), the simulation data indicate that the boundary parameter η_0 is fixed. Using the same fitting procedure as before, we obtain $h_-^{(3)} = -528.5$, $g_-^{(3)} = 11.0$ and $c^{(3)} = 0.1$. Once again, we omit the errors of the fit since they are several orders of magnitude higher than the obtained optimal parameters.

V. CONCLUSIONS

In the present work we study the boundary conditions at the surface of hydrophobic cone-shaped inclusions that are inserted into bilayer membranes by a combined analytic / simulation approach. For this, we describe the shape of a lipid double membrane perturbed by a conical inclusion in terms of a scalar order parameter according to Landau theory. From the minimization of the membrane elastic energy that is described by the Landau theory, we obtain theoretical predictions for the order parameter profile in the bulk and the order parameter value at the cone-membrane interface. We also perform all-atom MD simulations of a DMPC lipid bilayer that is perturbed by a hydrophobic conical inclusion of varying half opening angle and extract the displacement of the membrane middle plane, the membrane thickness, and the middle plane bending angle as scalar order parameters from our simulations. By comparison of the MD data with the predictions of the Landau theory, we fit all parameters in the phenomenological Landau theory for the boundary values of the order parameters.

For all our choices of order parameters, we clearly observe a perturbation of the membrane shape caused by the inclusion. However, the conical inclusions of different opening angles, and thus different sizes, do not produce significantly different perturbations in the surface values of the order parameters we studied. It is clearly seen that the membrane displacement and bending angle are best described by fixed values η_0. The membrane thickness shows a slight boundary value variation as a function of the cone opening angle. Though a theory considering fixed boundary fields h_- and g_- yields the numerically best fitting prediction, a fixed boundary parameter η_0 is the simpler and still rather accurate boundary condition.

This is a rather surprising results that shows that the opening angle of cone-like inclusion is not simply adopted by the surrounding membrane and shows that the boundary condition at the interface between an inclusion and a lipid bilayer is far from trivial. For the membrane thickness order parameter, the nearly constant thickness at the interface most likely reflects the molecular architecture of a lipid bilayer, which determines a preferred thickness independent of the inclusion geometry. Regarding the membrane bending angle, the nearly constant angle at the interface might be caused by repulsive forces be-

tween polar membrane head groups and the hydrophobic inclusion, which could be studied in more detailed simulation models in the future. In particular, the addition of polar groups to the upper and lower end of the inclusion, which match the polarity of the head groups of the membrane lipids, might improve the analysis of the order parameters considered in this work. For the bending angle profile a more general Landau free energy including a second-derivative curvature term might be more suitable, which would result in a more realistic description of the bending energy of a bilayer. To examine the dependence of the membrane boundary condition on the inclusion size in a more realistic model, it might be useful to consider in future simulations inclusions that correspond to truncated cones and vary the lateral size as well as the opening angle of the inclusion. Finally, feature extraction would certainly improve for larger simulation system sizes, which would allow the membrane to reach a truly relaxed state far away from the inclusion.

ACKNOWLEDGMENTS

This research has been funded by Deutsche Forschungsgemeinschaft (DFG) through grant CRC 1114 "Scaling Cascades in Complex Systems", Project Number 235221301, Project C02 "Interface dynamics: Bridging stochastic and hydrodynamic descriptions".

Appendix: Supplementary Figures

[1] B. Alberts, A. Johnson, J. Lewis, D. Morgan, M. Raff, K. Roberts, and P. Walter, *Molecular Biology of the Cell*, sixth ed. (Garland Science, 2015).
[2] H. T. McMahon and E. Boucrot, Membrane curvature at a glance, Journal of Cell Science **128**, 1065 (2015).
[3] I. K. Jarsch, F. Daste, and J. L. Gallop, Membrane curvature in cell biology: An integration of molecular mechanisms, Journal of Cell Biology **214**, 375 (2016).
[4] M. G. J. Ford, I. G. Mills, B. J. Peter, Y. Vallis, G. J. K. Praefcke, P. R. Evans, and H. T. McMahon, Curvature of clathrin-coated pits driven by epsin, Nature **419**, 361 (2002).
[5] I. Tsafrir, Y. Caspi, M.-A. Guedeau-Boudeville, T. Arzi, and J. Stavans, Budding and Tubulation in Highly Oblate Vesicles by Anchored Amphiphilic Molecules, Physical Review Letters **91**, 138102 (2003).
[6] B. Antonny, Membrane deformation by protein coats, Current Opinion in Cell Biology Membranes and organelles, **18**, 386 (2006).
[7] J. Zimmerberg and M. M. Kozlov, How proteins produce cellular membrane curvature, Nature Reviews Molecular Cell Biology **7**, 9 (2006).
[8] W. Römer, L. Berland, V. Chambon, K. Gaus, B. Windschiegl, D. Tenza, M. R. E. Aly, V. Fraisier, J.-C. Florent, D. Perrais, C. Lamaze, G. Raposo, C. Steinem, P. Sens, P. Bassereau, and L. Johannes, Shiga toxin induces tubular membrane invaginations for its uptake into cells, Nature **450**, 670 (2007).
[9] S. M. Hashemi, P. Sens, and F. Mohammad-Rafiee, Regulation of the membrane wrapping transition of a cylindrical target by cytoskeleton adhesion, Journal of The Royal Society Interface **11**, 20140769 (2014).
[10] A. Arkhipov, Y. Yin, and K. Schulten, Four-Scale Description of Membrane Sculpting by BAR Domains, Biophysical Journal **95**, 2806 (2008).
[11] F. Campelo, H. T. McMahon, and M. M. Kozlov, The Hydrophobic Insertion Mechanism of Membrane Curvature Generation by Proteins, Biophysical Journal **95**, 2325 (2008).
[12] M. M. Kozlov, H. T. McMahon, and L. V. Chernomordik, Protein-driven membrane stresses in fusion and fission, Trends in Biochemical Sciences **35**, 699 (2010).
[13] P. B. Canham, The minimum energy of bending as a possible explanation of the biconcave shape of the human red blood cell, Journal of Theoretical Biology **26**, 61 (1970).
[14] W. Helfrich, Elastic Properties of Lipid Bilayers: Theory and Possible Experiments, Zeitschrift für Naturforschung C **28**, 693 (1973).
[15] F. Campelo, C. Arnarez, S. J. Marrink, and M. M. Kozlov, Helfrich model of membrane bending: From Gibbs theory of liquid interfaces to membranes as thick anisotropic elastic layers, Advances in Colloid and Interface Science Special issue in honour of Wolfgang Helfrich, **208**, 25 (2014).
[16] M. Deserno, Fluid lipid membranes: From differential geometry to curvature stresses, Chemistry and Physics of Lipids Membrane mechanochemistry: From the molecular to the cellular scale, **185**, 11 (2015).
[17] R. Lipowsky, Budding of membranes induced by intramembrane domains, Journal de Physique II **2**, 1825 (1992).
[18] F. Jülicher and R. Lipowsky, Shape transformations of vesicles with intramembrane domains, Physical Review E **53**, 2670 (1996).
[19] R. R. Netz, Inclusions in Fluctuating Membranes: Exact Results, Journal de Physique I **7**, 833 (1997).
[20] T. R. Weikl, M. M. Kozlov, and W. Helfrich, Interaction of conical membrane inclusions: Effect of lateral tension, Physical Review E **57**, 6988 (1998).
[21] T. Kies and C. Gräser, On differentiability of the membrane-mediated mechanical interaction energy of discrete-continuum membrane-particle models, arXiv:1711.11192 [math] (2021).
[22] C. M. Elliott, C. Gräser, G. Hobbs, R. Kornhuber, and M.-W. Wolf, A Variational Approach to Particles in Lipid Membranes, Archive for Rational Mechanics and Analysis **222**, 1011 (2016).
[23] L. Landau, Zur Theorie der Phasenumwandlungen II, Physikalische Zeitschrift der Sowjetunion **11**, 26 (1937).
[24] S. Marčelja and N. Radić, Repulsion of interfaces due to boundary water, Chemical Physics Letters **42**, 129 (1976).
[25] C.-M. Chen, T. C. Lubensky, and F. C. MacKintosh, Phase transitions and modulated phases in lipid bilayers,

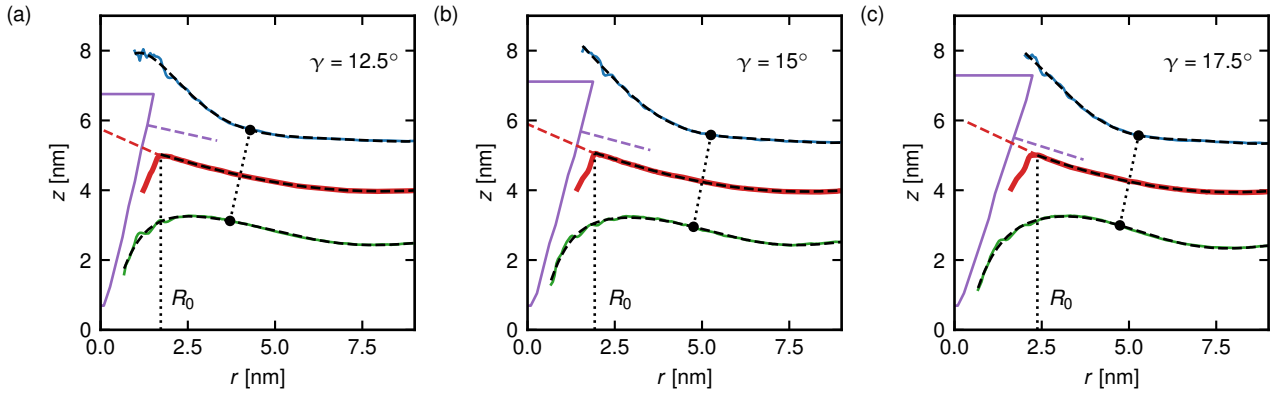

FIG. 5. Radial membrane profiles for $\gamma = 12.5°$ (a), $\gamma = 15°$ (b) and $\gamma = 17.5°$ (c) from MD simulations. Extracted radial averages of the upper and lower leaflet head group positions as well as the middle plane positions are shown as solid lines in color: upper leaflet head group position in blue, lower leaflet head group position in green, and middle plane position in red. A tangent to the middle plane profile at the cone-membrane interface R_0 is shown by a red dashed line. The corresponding polynomial fits are shown as black dashed lines. The conical inclusion is represented by a solid purple line through the outermost atoms' centers of the cone. The purple dashed line is orthogonal to the cone edge profile as a guide to the eye. The lipid cone interface at R_0 is indicated by a black dotted vertical line. The orthogonal projection to the middle plane profile is shown by a black dotted line, where black filled circles indicate the extracted membrane thickness.

Physical Review E **51**, 504 (1995).

[26] J.-B. Fournier, Microscopic membrane elasticity and interactions among membrane inclusions: interplay between the shape, dilation, tilt and tilt-difference modes, The European Physical Journal B - Condensed Matter and Complex Systems **11**, 261 (1999).

[27] M. Kanduč, A. Schlaich, E. Schneck, and R. R. Netz, Hydration repulsion between membranes and polar surfaces: Simulation approaches versus continuum theories, Advances in Colloid and Interface Science Special issue in honour of Wolfgang Helfrich, **208**, 142 (2014).

[28] A. Schlaich, B. Kowalik, M. Kanduč, E. Schneck, and R. R. Netz, Physical mechanisms of the interaction between lipid membranes in the aqueous environment, Physica A: Statistical Mechanics and its Applications Proceedings of the 13th International Summer School on Fundamental Problems in Statistical Physics, **418**, 105 (2015).

[29] T. Auth and G. Gompper, Budding and vesiculation induced by conical membrane inclusions, Physical Review E **80**, 031901 (2009).

[30] J.-B. Fournier and P. Galatola, High-order power series expansion of the elastic interaction between conical membrane inclusions, The European Physical Journal E **38**, 86 (2015).

[31] R. B. Best, X. Zhu, J. Shim, P. E. M. Lopes, J. Mittal, M. Feig, and A. D. MacKerell, Optimization of the Additive CHARMM All-Atom Protein Force Field Targeting Improved Sampling of the Backbone ϕ, ψ and Side-Chain χ_1 and χ_2 Dihedral Angles, Journal of Chemical Theory and Computation **8**, 3257 (2012).

[32] G. Bussi, D. Donadio, and M. Parrinello, Canonical Sampling through Velocity Rescaling, The Journal of Chemical Physics **126**, 014101 (2007).

[33] H. J. C. Berendsen, J. P. M. Postma, W. F. van Gunsteren, A. DiNola, and J. R. Haak, Molecular Dynamics with Coupling to an External Bath, The Journal of Chemical Physics **81**, 3684 (1984).